Progress In Electromagnetics Research C, Vol. 101, 173–186, 2020

2-D Analytical Model for Slotless Double-Sided Outer Armature Permanent-Magnet Linear Motor

Alireza Ghaffari[1, *], Farzaneh Khalili[2], Amir A. Vahaj[1], Hamidreza Ghaffari[1], and Amin Mahmoudi[3]

Abstract—Slotless double-sided outer armature permanent-magnet (PM) linear motors (SDOPMLs) have high efficiency and low detent force. Despite their simple control strategy and easy manufacturing process, finding an accurate model of these motors to calculate the machine quantities is challenging. It is particularly critical for obtaining the optimum design of these machines which may include too many iterations in a short time. To overcome this challenge, a 2-D analytical model based on the sub-domain method is presented to determine the magnetic flux density components for the motor under the study. According to this analytical procedure, the motor cross-section is divided to 11 sub-regions, then the superposition theorem is utilized to analyze the flux density distribution in all sub-regions due to various magnetization patterns, (i.e., parallel, two-segment Halbach, ideal Halbach, and bar magnet in shifting directions) as well as armature reaction current, respectively. According to the calculated magnetic flux density components, machine quantities like flux linkage, induced voltage, inductances, and electromagnetic force components are explained. Also, the obtained analytical results are compared with those of the finite-element method (FEM) to confirm the accuracy of the proposed model. The proposed model can be used in the design and optimization stage of the linear slotless motor against the numerical model to save time. Finally, a comparative study between the performance of the single-sided and double-sided slotless PM linear motors in the same volume is implemented. This comparison shows the advantage of the double-sided motor in terms of the unbalanced magnetic force (UMF).

1. INTRODUCTION

Many modern medical technologies employ linear motion, resulting in the need for stable and high performing linear motors [1]. PM and induction linear motors are two prevalent types of linear motors, and PM linear motors generally have a high efficiency compared to induction motor [2]. PM linear motors organize many different fabrications for the mover and stator, which are intended for reducing expenses, volume, and losses. The stators of PM linear motors have either a slotted or a slotless structure. The slotless one has higher accuracy and better heat exchange than the slotted design due to windings exposure to the air near the motor circumference. The mentioned advantages explain the prevalent use of slotless double-sided outer armature permanent magnet linear motors in many applications [3].

The fundamental benefit of a double-sided stator structure rather than the single-sided one is the separated magnetization patterns, which allow for magnetic flux lines to pass through the mover without the need of ferrite material (except for the parallel magnetization pattern in which PMs in both sides are magnetized oppositely). It could result in a coreless mover which reduces the iron loss, cost, and weight in the linear machines.

Received 21 January 2020, Accepted 16 April 2020, Scheduled 30 April 2020

* Corresponding author: Alireza Ghaffari (a.ghaffari@sutech.ac.ir).

[1] Department of Electrical and Electronics Engineering, Shiraz University of Technology, Shiraz 71557-13876, Iran. [2] Department of Mathematic, Shiraz University of Technology, Shiraz 71557-13876, Iran. [3] College of Science and Engineering, Flinders University, Adelaide, SA 5042, Australia.

Analytical and numerical models are defined as two basic models for analyzing electrical machines. The numerical methods, such as FEM, have high accuracy, and these methods are useful for considering geometric details and the nonlinearity of magnetic material. However, it has a high computational time and consequently not suitable in the primary design stages. Therefore, analytical models, if possible, are preferred in the primary design stages to estimate the performance of electrical motors because of three privileges. Firstly, it is faster than FEM which is essential for the optimization issues with numerous iterations. Secondly, the analytical method provides a better understanding of the system. It helps to comprehend governing equations in the electrical machines. Ultimately, the analytical model is more flexible for modifying motor specifications, such as the dimensions of motor or the number of PMs, in spite of the numerical methods in which changing the specifications requires remodeling the machine.

Several analytical models of electrical machines have been presented in recent years [4–27]. For instance, [4] presented a quasi-three-dimensional (3-D) analytical model of the magnetic field in an axial flux permanent-magnet synchronous machine, and in the obtained model the core permeability was assumed infinite. Also the model was limited to the specific magnetization pattern. Only the PM effects were considered, and armature current effects on the flux density distribution were not analyzed. Kang et al. [6] proposed an electromagnetic model for an air-core type PM linear motor based on space harmonics field and equivalent magnetizing current model to acquire the force and back-emf. However, the permeability of back iron was considered to be infinite, and various magnetization patterns were not investigated. Furthermore, Vaez-Zadeh and Isfahani [7] analyzed the performance characteristics of an air-core linear PM synchronous motor by varying motor design parameters in a layer and d-q model of the machine to improve thrust and reduce thrust ripple and PMs volume in which the core permeability was assumed to be infinite. Also, their model did not consider alternate magnetization patterns. Additionally, Vaez-Zadeh and Isfahani [9] described an alternative method to model the air-gap flux density distribution which is both accurate and simple enough to be integrated into iterative motor design procedures. In their model, calculations of performance quantities were limited to the magnetic flux and magnetic force for the parallel magnetization pattern, and other quantities such as induced voltage and inductances were not expressed. A general analytical model was proposed in [11] to calculate the back electromotive forces of various manufacturing imperfections in the double rotor axial flux permanent magnet machine in which the core permeability was assumed to be infinite, and flux density was originated due to only PMs, and the effects of armature currents on the flux density distribution were not considered. A 2D analytical solution for predicting the magnetic field distribution in ironless BLDC motor was presented in [19]. The back iron permeability was assumed to be infinite, and armature reaction effects were not analyzed. Brahim et al. [21] proposed an analytical model of the electrical motor for predicting the magnetic flux distribution based on the equivalent magnetization intensity method, but this model did not investigate armature current effects. Eventually, an analytical model for a double-sided air-core permanent magnet linear servo motor with trapezoidal shape permanent magnets was proposed in [27]. For simplifying the related equations the permeability of cores was assumed to be infinite, and the analytical model was expressed for a specified magnetization pattern.

According to the literature review, a limited number of papers investigated the analytical model for estimating the machine quantities due to both armature reaction and various magnetization patterns including finite-permeability for cores, simultaneously. For this purpose, the sub-domain method is implemented to governing partial differential equations (PDEs) by applying Maxwell's equations in each sub-region.

The primary contribution of this paper is to obtain a highly accurate two-dimensional analytical model based on the sub-domain method for SDOPML by considering the finite permeability of the cores, which calculates flux density components. Various magnetization patterns (i.e., parallel, ideal Halbach, 2-segment Halbach, and bar magnet in shifting direction), as well as armature currents, are investigated to estimate the main machine quantities such as flux density components, inductances, flux linkage, induced voltage, and electromagnetic force components. Finally, FEM results are utilized to verify the deduced analytical model. Moreover, a comparison between single and double-sided slotless linear motors in the same volume is applied to reveal the elimination of UMF with a small reduction of the output power.

2. STRUCTURE AND ASSUMPTIONS

Figure 1 presents the proposed SDOPML for obtaining the analytical model based on the sub-domain method. In this method, the machine cross-section is divided into 11 sub-regions: primary stator exterior (*pse*), primary stator (*ps*), primary winding (*pw*), primary air-gap (*pa*), primary permanent magnet (*ppm*), mover (*m*), secondary permanent magnet (*spm*), secondary air-gap (*sa*), secondary winding (*sw*), secondary stator (*ss*), and secondary stator exterior (*sse*). The magnetic vector potential is determined by solving Maxwell equations in each sub-region. Finally, applying curl on the derived magnetic vector potential leads to obtaining the normal and tangential components of the magnetic flux density components. It is noted that magnetic flux density components, due to PMs and armature current, are obtained respectively, then the superposition theorem is utilized to express the total magnetic flux density components. The proposed 2-D analytical model is based on the following assumptions:

i. The motor has an infinite length in the x-direction.
ii. The magnetic flux density vector in each sub-region is independent of z and z-axis.
iii. The saturation effect is ignored.
iv. The current density vectors have only a component in the z-direction.
v. The eddy current reaction is ignored.

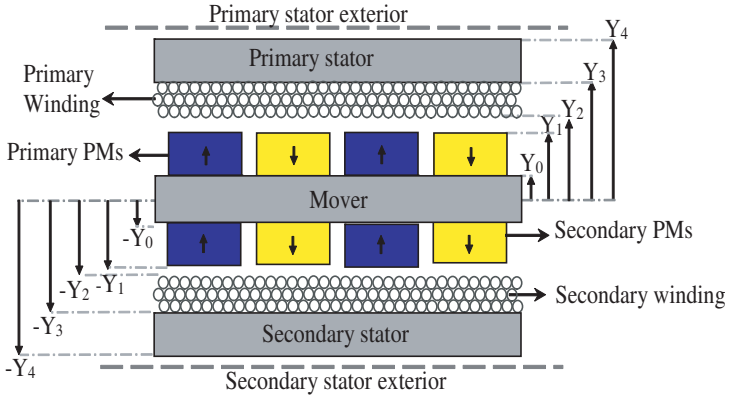

Figure 1. Structure and sub-region of the proposed SDOPML.

3. MAGNETIC FLUX DENSITY COMPONENTS

3.1. Armature Reaction Currents

To obtain the analytical model of the magnetic field distribution due to the only armature currents, PMs remanence flux is forced to zero. In this part, all of the sub-regions are divided into two types of sub-domains. The first type (i) includes *pse*, *ps*, *pa*, *ppm*, *m*, *spm*, *sa*, *ss*, and *sse* sub-regions in which the Maxwell equations for these sub-regions are Laplace equations as:

$$\frac{\partial^2 A_z^i}{\partial^2 x} + \frac{\partial^2 A_z^i}{\partial^2 y} = 0 \quad i = pse, ps, pa, ppm, m, spm, sa, ss, sse \tag{1}$$

The second type of the sub-domains (w) consists of *pw* and *sw* sub-regions, and the applied currents in these two sub-regions are presented as follows:

$$i_j(t) = \sum_k I_k \sin\left(k\left(p\frac{v}{L_x}\pi t - \frac{2\pi\,(j-1)}{q}\right) + \theta_k\right), \quad j = 1, 2, \ldots, q \tag{2}$$

In spite of the first type of sub-regions the corresponding PDEs in both winding sub-regions are the Poisson one proposed as follows:

$$\frac{\partial^2 A_z^w}{\partial x^2} + \frac{\partial^2 A_z^w}{\partial y^2} = -\mu_0 \mathbf{J}, \tag{3}$$

J is determined by its Fourier series expansion as follows:

$$\mathbf{J} = \sum_{n=1}^{\infty} \left[J_{1n} \sin(\alpha_n x) + J_{2n} \cos(\alpha_n x) \right] \tag{4}$$

where $\alpha_n = n\pi/\tau_p$. For a q-phases motor, J_{1n} and J_{2n} are defined by their Fourier series expansion coefficients which are obtained as follows:

$$\begin{aligned} J_{1n} &= -\frac{2N_t}{\frac{\tau_p}{3}(y_3 - y_2)} \frac{\cos\left(\frac{(q+1)n\pi}{2q}\right) - \cos\left(\frac{(q-1)n\pi}{2q}\right)}{n\pi} \\ &\times \left[i_s(t) + \sum_{\substack{r=1 \\ r\neq s}}^{(q-1)/2} i_r(t) \cos\left(\frac{(q-r)n\pi}{q}\right) + \sum_{\substack{w=1, \\ w\neq s}}^{(q-1)/2} i_w(t) \cos\left(\frac{(q+w)n\pi}{q}\right) \right] \end{aligned} \tag{5}$$

$$J_{2n} = -\frac{2N_t}{\frac{\tau_p}{3}(y_3 - y_2)} \frac{\cos\left(\frac{(q+1)n\pi}{2q}\right) - \cos\left(\frac{(q-1)n\pi}{2q}\right)}{n\pi} \times \sum_{j=1}^{q} i_j(t) \sin\left(\frac{2(j-1)n\pi}{q}\right) \tag{6}$$

where s is the phase by symmetrical distribution with respect to the z-axis.

The separation of variables method is utilized to calculate the general solution of Laplace's and Poisson's equations. Imposing the curl on the calculated magnetic vector potential leads to concluding the following equations for the magnetic flux density in i and w sub-regions:

$$B_x^i = \sum_{n=1}^{N} \alpha_n \left(a_n^i \cosh(\alpha_n y) + b_n^i \sinh(\alpha_n y) \right) \cos(\alpha_n x) + \alpha_n \left(c_n^i \cosh(\alpha_n y) + d_n^i \sinh(\alpha_n y) \right) \sin(\alpha_n x) \tag{7}$$

$$B_y^i = \sum_{n=1}^{N} \alpha_n (a_n^i \sinh(\alpha_n y) + b_n^i \cosh(\alpha_n y)) \sin(\alpha_n x) - \alpha_n \left(c_n^i c \sinh(\alpha_n y) + d_n^i \cosh(\alpha_n y) \right) \cos(\alpha_n x) \tag{8}$$

$$B_x^w = \sum_{n=1}^{N} \alpha_n (a_n^w \cosh(\alpha_n y) + b_n^w \sinh(\alpha_n y)) \cos(\alpha_n x) + \alpha_n (c_n^w \cosh(\alpha_n y) + d_n^w \sinh(\alpha_n y)) \sin \alpha_n(x) \tag{9}$$

$$\begin{aligned} B_y^w = &\sum_{n=1}^{N} \alpha_n \left(a_n^w \sinh(\alpha_n y) + b_n^w \cosh(\alpha_n y) + \frac{\mu_0 J_{2n}}{\alpha_n^2} \right) \sin(\alpha_n x) \\ &-\alpha_n \left(c_n^w \sinh(\alpha_n y) + d_n^w \cosh(\alpha_n y) + \frac{\mu_0 J_{1n}}{\alpha_n^2} \right) \cos(\alpha_n x) \end{aligned} \tag{10}$$

3.2. Magnetic Flux Density Due to PMs

To consider the flux density originated by only PMs, armature currents are set to zero. At this stage, similar to the previous section, all sub-regions are divided into two types of sub-region. The first type consists of *pse*, *ps*, *pw*, *pa*, *m*, *sa*, *sw*, *ss*, and *sse*. The second type of sub-regions includes *ppm* and *spm* sub-regions. In this step, the first and second types of sub-regions are denoted by superscripts f and *pm*, respectively. Laplace's and Poisson's equations for magnetic vector potential in each sub-region due to the PMs can be expressed as:

$$\frac{\partial^2 A_z^f}{\partial x^2} + \frac{\partial^2 A_z^f}{\partial y^2} = 0, \quad f = pse,\ ps,\ pw,\ pa,\ m,\ sa,\ sw,\ ss,\ sse \tag{11}$$

$$\frac{\partial^2 A_z^{pm}}{\partial x^2} + \frac{\partial^2 A_z^{pm}}{\partial y^2} = -\mu_0 \left(\frac{\partial M_y}{\partial x} - \frac{\partial M_x}{\partial y} \right), \quad p = ppm,\ spm \tag{12}$$

M is written as:

$$\mathbf{M} = M_x a_x + M_y a_y \tag{13}$$

To solve the PDEs originated by only PMs, it is helpful to know the magnetization vector components. The related components of magnetization vector patterns for the parallel magnetization patterns are presented as:

$$m_{xn} = 0 \tag{14}$$

$$m_{yn} = \frac{4B_{rem}}{\mu_0 n\pi} \sin(n\pi/2) \sin(\alpha_n \tau_m/2) \tag{15}$$

In an ideal Halbach magnetization pattern, these coefficients can be easily written as follows:

$$m_{xn} = \begin{cases} B_{rem}/\mu_0 & \text{for } n = 1 \\ 0 & \text{otherwise} \end{cases} \tag{16}$$

$$m_{yn} = \begin{cases} -B_{rem}/\mu_0 & \text{for } n = 1 \\ 0 & \text{otherwise} \end{cases} \tag{17}$$

Those for the 2-segment Halbach magnetization pattern can be expressed as:

$$m_{xn} = -\frac{4B_{rem}}{\mu_0 n\pi} \sin(n\pi\, k_x/2) \tag{18}$$

$$m_{yn} = -\frac{2B_{rem}}{\mu_0 n\pi} \left[\cos(n\pi\,(k_x/2 + k_y)) - \cos(n\pi\, k_x/2)\right] \tag{19}$$

Finally, Fourier series expansion coefficients for the bar magnets in shifting direction magnetization pattern are obtained as:

$$m_{xn} = \begin{cases} -\dfrac{4n\alpha_p^2 B_{rem}}{\mu_0 \pi} \dfrac{\sin\left(\frac{n\pi}{2}\right) \cos\left(\frac{n\pi\alpha_p}{2}\right)}{1 - (n\alpha_p)^2} & n\alpha_p \neq 1 \\ -\dfrac{B_{rem}}{n\mu_0} & n\alpha_p = 1 \end{cases} \tag{20}$$

$$m_{yn} = \begin{cases} \dfrac{4n\alpha_p B_{rem}}{\mu_0 \pi} \dfrac{\sin\left(\frac{n\pi}{2}\right) \cos\left(\frac{n\pi\alpha_p}{2}\right)}{1 - (n\alpha_p)^2} & n\alpha_p \neq 1 \\ \dfrac{B_{rem}}{n\mu_0} & n\alpha_p = 1 \end{cases} \tag{21}$$

where $\alpha_p = \frac{\tau_m}{\tau_p}$. Utilizing the separation of variables method as well as curl operation leads to extracting the following magnetic flux density relations:

$$\begin{aligned} B_x^f = &\sum_{n=1}^{N} \alpha_n \left(a_n^f \cosh(\alpha_n y) + b_n^f \sinh(\alpha_n y)\right) \cos(\alpha_n x) \\ &+ \alpha_n \left(c_n^f \cosh(\alpha_n y) + d_n^f \sinh(\alpha_n y)\right) \sin \alpha_n(x) \end{aligned} \tag{22}$$

$$\begin{aligned} B_y^f = &\sum_{n=1}^{N} \alpha_n \left(a_n^f \sinh(\alpha_n y) + b_n^f \cosh(\alpha_n y)\right) \sin(\alpha_n x) \\ &- \alpha_n \left(c_n^f \sinh(\alpha_n y) + d_n^f \cosh(\alpha_n y)\right) \cos(\alpha_n x) \end{aligned} \tag{23}$$

$$\begin{aligned} B_x^{pm} = &\sum_{n=1}^{N} \alpha_n (a_n^{pm} \cosh(\alpha_n y) + b_n^{pm} \sinh(\alpha_n y)) \cos(\alpha_n x) \\ &+ \alpha_n (c_n^{pm} \cosh(\alpha_n y) + d_n^{pm} \sinh(\alpha_n y)) \sin \alpha_n(x) \end{aligned} \tag{24}$$

$$\begin{aligned} B_y^{pm} = &\sum_{n=1}^{N} \alpha_n \left(a_n^{pm} \sinh(\alpha_n y) + b_n^{pm} \cosh(\alpha_n y)\right) \sin(\alpha_n x) \\ &- \alpha_n \left[(c_n^{pm} \sinh(\alpha_n y) + d_n^{pm} \cosh(\alpha_n y)) \cos \alpha_n(x)\right] + \mu_0 m_{yn} \sin(\alpha_n x) \end{aligned} \tag{25}$$

For considering the motion of mover, x in the particular solution of Eqs. (24)–(25) is replaced by $x - d$ in which d is defined as follows:

$$d = vt + d_0 \tag{26}$$

3.3. Boundary Conditions

Boundary conditions are applied to determine unknown coefficients of the magnetic vector potential. Boundary conditions for SDOPML are listed in Table 1 in which normal components of magnetic flux density ($B_\perp$) and tangential components of magnetic field intensity ($H_{||}$) must continue in the interface between two adjacent sub-regions. These boundary conditions are defined as:

$$H_x^i(x,y)\,|_{y=Y} = H_x^{i+}(x,y)\,|_{y=Y} \tag{27}$$

$$(i, i^+, Y) = \{(pse, ps, y_4), (ps, pw, y_3), (pw, pa, y_2), (pa, ppm, y_1), (ppm, m, y_0), (spm, m, -y_0), (sa, spm, -y_1), (sw, sa, -y_2), (ss, sw, -y_3), (sse, ss, -y_4)\}$$

$$B_y^i(x,y)\,|_{y=Y} = B_y^{i+}(x,y)\,|_{y=Y} \tag{28}$$

Applying the boundary conditions leads to obtaining 40 equations and 40 variables as b_n^{pse}, d_n^{pse}, a_n^{ps}, b_n^{ps}, c_n^{ps}, d_n^{ps}, a_n^{pw}, b_n^{pw}, c_n^{pw}, d_n^{pw}, a_n^{pa}, b_n^{pa}, c_n^{pa}, d_n^{pa}, a_n^{ppm}, b_n^{ppm}, c_n^{ppm}, d_n^{ppm}, a_n^{m}, b_n^{m}, c_n^{m}, d_n^{m}, a_n^{spm}, b_n^{spm}, c_n^{spm}, d_n^{spm}, a_n^{sa}, b_n^{sa}, c_n^{sa}, d_n^{sa}, a_n^{sw}, b_n^{sw}, c_n^{sw}, d_n^{sw}, a_n^{ss}, b_n^{ss}, c_n^{ss}, d_n^{ss}, a_n^{sse}, c_n^{sse}. It is noted that to have reasonable results some of the coefficients (i.e., a_n^{pse}, c_n^{pse}, b_n^{sse}, d_n^{sse}) must be zero [28].

Table 1. Boundary conditions in the motor under the study.

Adjacent sub-regions	Boundary conditions
Primary stator exterior and primary stator in $y = y_4$	$H_x^{pse} = H_x^{ps}$ $B_y^{pse} = B_y^{ps}$
Primary stator and primary winding in $y = y_3$	$H_x^{ps} = H_x^{pw}$ $B_y^{ps} = B_y^{pw}$
Primary winding and primary air-gap in $y = y_2$	$H_x^{pw} = H_x^{pa}$ $B_y^{pw} = B_y^{pa}$
Primary air-gap and primary PM in $y = y_1$	$H_x^{pa} = H_x^{ppm}$ $B_y^{pa} = B_y^{ppm}$
Primary PMs and Mover in $y = y_0$	$H_x^{ppm} = H_x^{m}$ $B_y^{ppm} = B_y^{m}$
Mover and secondary PMs in $y = -y_0$	$H_x^{m} = H_x^{spm}$ $B_y^{m} = B_y^{spm}$
Secondary PMs and secondary air-gap in $y = -y_1$	$H_x^{spm} = H_x^{sa}$ $B_y^{spm} = B_y^{sa}$
Secondary air-gap and secondary winding in $y = -y_2$	$H_x^{sa} = H_x^{sw}$ $B_y^{sa} = B_y^{sw}$
Secondary winding and secondary stator in $y = -y_3$	$H_x^{sw} = H_x^{ss}$ $B_y^{sw} = B_y^{ss}$
Secondary stator and secondary stator exterior in $y = -y_4$	$H_x^{ss} = H_x^{sse}$ $B_y^{ss} = B_y^{sse}$

4. CASE STUDY

4.1. Magnetic Flux Density

Based on dimensional and geometry data which are listed in Table 2, the straightforward comparison between the proposed analytical model and FEM is carried out for the motor under study to validate the accuracy of the presented analytical model. The analytical model has the flexibility (compared to the numerical one) in modifying the motor specifications (e.g., velocity, and dimensions). So, there is no difficulty in implementing different values of Table 2 to estimate the output quantities. Figures 2 and 3 compare the analytical and FEM results of the magnetic flux density components originated by PMs and armature reaction, respectively. It is evident that an acceptable accuracy is observed between the FEM and proposed analytical models. Based on the magnetization patterns on both sides of the proposed motor, tangential components of magnetic flux density in the mover due to the Halbach magnetization patterns are not considerable. Therefore, it is possible to replace suitable materials instead of steel for the mover to reduce the volume, core losses, and cost. It is seen that the components of flux density originated by ideal Halbach magnetization pattern include lower harmonic compared with the extracted results of the other magnetization patterns.

Table 2. Specifications of the investigated SDOPML.

Symbols	Values	Symbols	Values
L_x	200 mm	p	4
y_0	5 mm	L_z	50 mm
$y_1 - y_0$	4 mm	k_x	0.4
$y_2 - y_1$	1 mm	k_y	0.6
$y_3 - y_2$	5 mm	B_{rem}	1.23 T
$y_4 - y_3$	5 mm	I_m	5 A
μ_r^s	1000	N_t	41
μ_r^m	1000	N_c	4
μ_r^{pm}	1.1	K_f	0.6
τ_m	40 mm	v	1 m/s
τ_p	50 mm		

4.2. Inductances

To calculate the self and mutual inductances, it is necessary to find linked magnetic flux density by winding sub-region which is originated by only armature reaction currents. This linkage flux is calculated as follows:

$$\lambda_i^w = N_t N_c \int \mathbf{B^w} \cdot d\mathbf{s} = N_t N_c L_z \int_{x1}^{x2} B_y^w dx \tag{29}$$

where B_y^w should be originated due to the only armature currents. According to the obtained flux linkage, the self-inductances can be defined as follows:

$$L_{ii} = \frac{\lambda_i^w}{I_i} \tag{30}$$

Also, the mutual inductance is presented as:

$$L_{ij} = \frac{\lambda_{ij}^w}{I_i} \tag{31}$$

Neglecting the saturation effects causes the calculated inductance independent of armature currents, and it mostly depends on the length of air-gap. Therefore, self and mutual inductances are constant

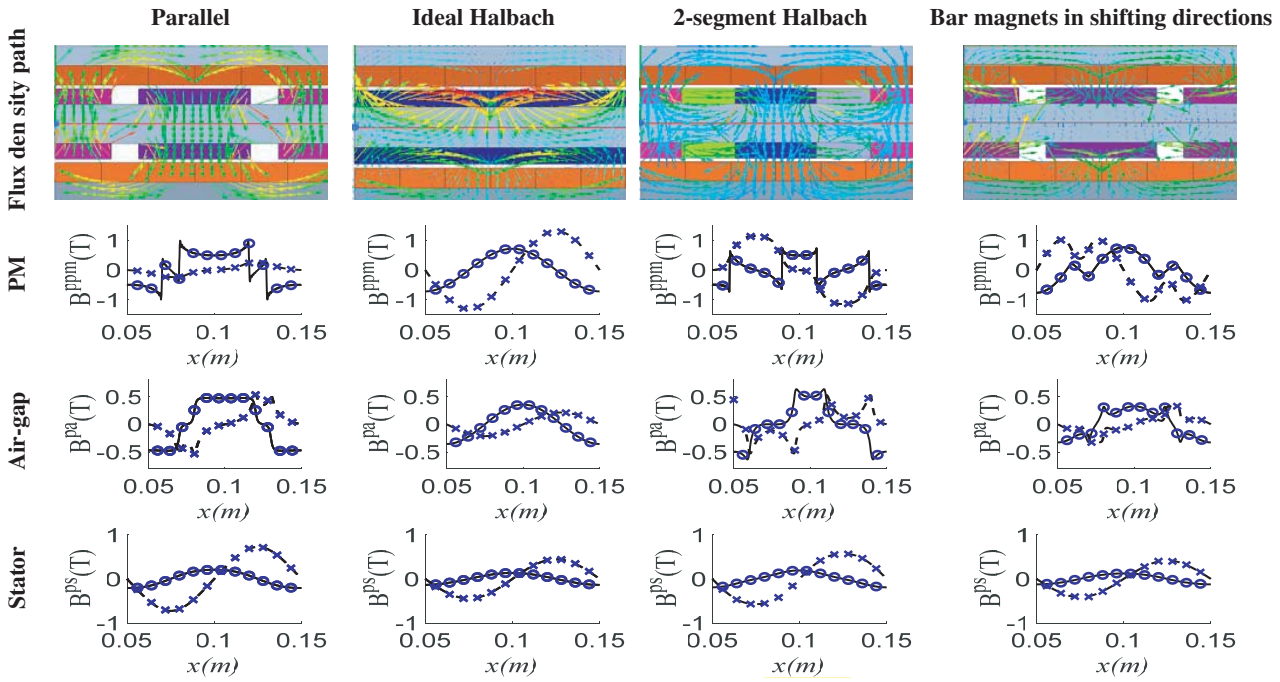

(a): Primary sub-regions of the proposed SDOPML

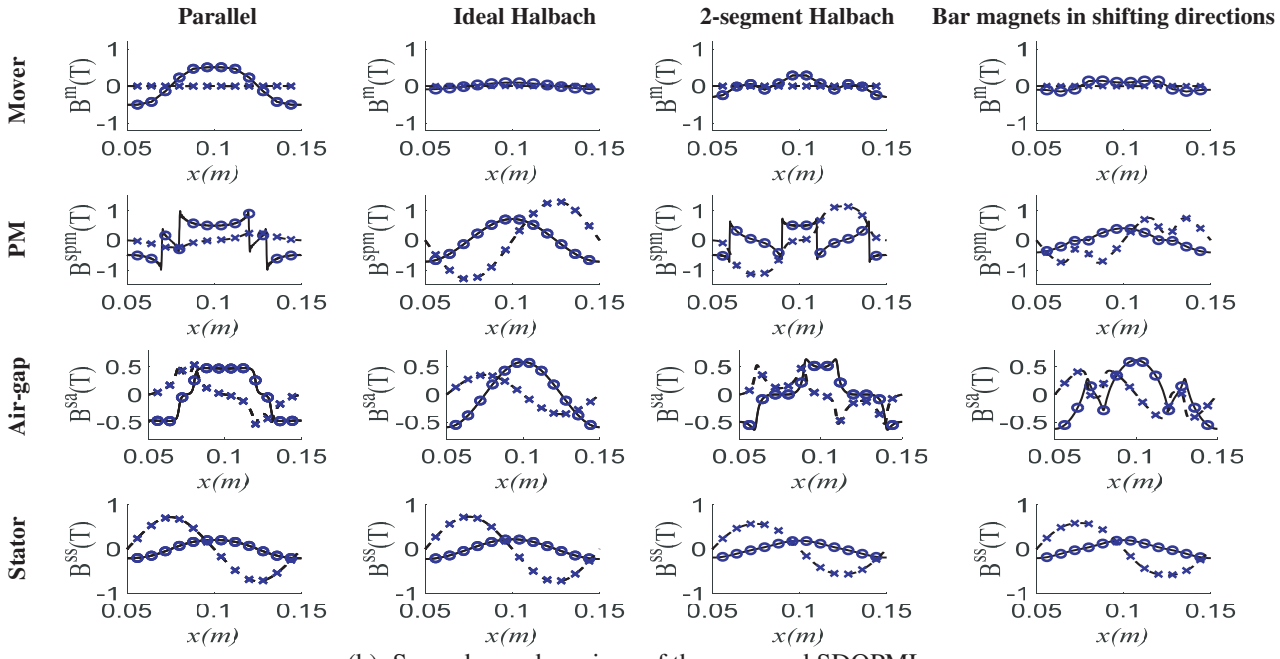

(b): Secondary sub-regions of the proposed SDOPML

o Numerical results of the normal component of flux density
× Numerical results of the tangential component of flux density
- - Analytical results of the tangential components of flux density
— Analytical results of the normal component of flux density

Figure 2. Analytical and numerical results of flux density distribution due to only PMs in the motor under the study.

due to the constant magnetic air-gap in the proposed slotless motor including surface mounted PMs. The analytical and numerical results of the self and mutual inductances for the proposed motor are determined in Table 3.

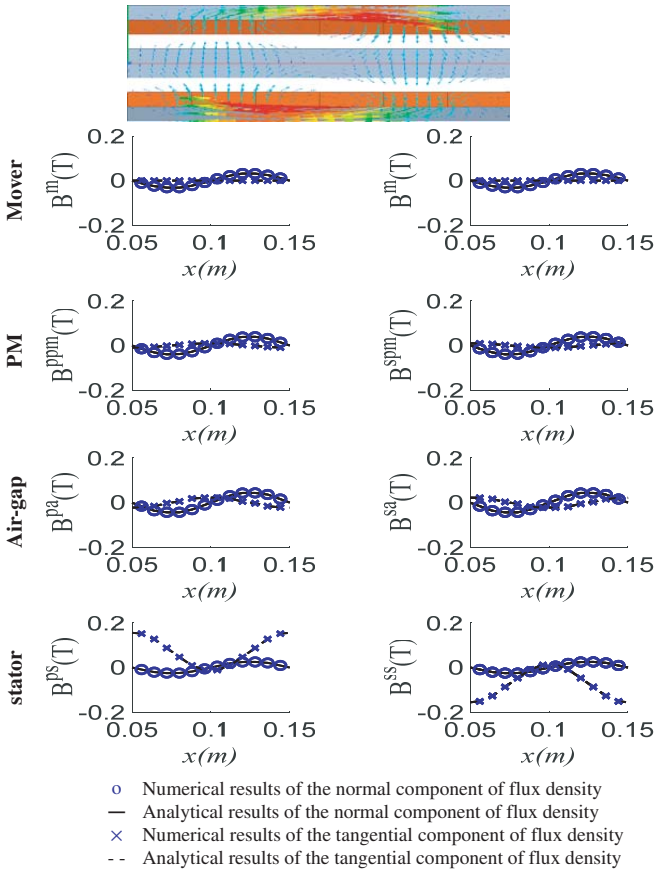

Figure 3. Flux density distribution due to only armature reaction for the motor under the study.

Table 3. Inductances for the proposed SDOPML.

	2-D Analytical	2-D FEM
Self-inductance (mH)	1.51	1.54
Mutual-inductance (mH)	0.74	0.78

4.3. Induced Voltage

According to Faraday's law, the ratio of the flux linkage changes, originated by PMs, to time changes is defined as the induced voltage. This definition can be expressed as:

$$E_i = -\frac{d\lambda_i^{pm}}{dt} \tag{32}$$

Figure 4 illustrates the defined induced voltage due to the various proposed magnetization patterns in this paper.

4.4. Total Harmonic Distortion (THD)

The analytical model completely depends on the maximum value of $n(N)$. It means that N in the obtained magnetic vector potential equations in each sub-region plays an important role in calculating the THD and defining the accuracy of the proposed analytical model. Table 4 expresses the effect of this value on the THD of the induced voltage for the various investigated magnetization patterns. Based on the calculated THD, N for the motor under the study is assumed 150.

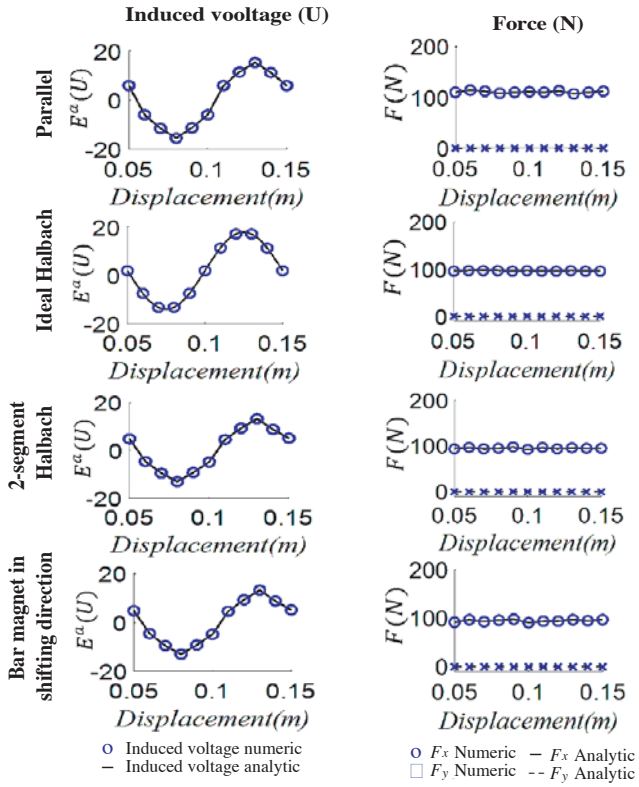

Figure 4. Induced voltage, flux linkage, Normal and tangential force component for the proposed SDOPML.

Table 4. Effect of the maximum harmonic orders of the magnetic vector potential on induced voltage THD%.

Magnetization pattern	$N = 5$	$N = 10$	$N = 20$	$N = 30$	$N = 50$	$N = 100$	$N = 150$	$N = 200$
Parallel	73%	41%	30%	24%	19%	11%	9%	7%
Ideal Halbach	58%	28%	19%	14%	11%	4%	3%	2%
2-Segment Halbach	67%	32%	28%	21%	15%	6%	4%	3%
Bar magnet in shifting direction	69%	34%	29%	23%	16%	7%	6%	4%

4.5. Electromagnetic Force Components

Maxwell's stress tensor method is utilized to calculate the normal and tangential components of the electromagnetic force components. Flux density distributions in both primary and secondary air-gaps in the proposed SDOPML play important roles for calculating force components as follows:

$$F_x = \frac{L_z}{\mu_0} \int_{\frac{-L_x}{2}}^{\frac{L_x}{2}} [B_x^{pa} B_y^{pa} + B_x^{sa} B_y^{sa}] dx \tag{33}$$

$$F_y = \frac{L_z}{2\mu_0} \int_{\frac{-L_x}{2}}^{\frac{L_x}{2}} \left([B_x^{pa}]^2 - [B_y^{pa}]^2 \right) + \left([B_x^{sa}]^2 - [B_y^{sa}]^2 \right) dx \tag{34}$$

Analytical and numerical results of the normal and tangential components of the electromagnetic force are shown in Figure 4.

The fascinating advantage of the analytical models is their simulation time. A maximum length of 4 mm in each mesh was assumed for the FEM model, and analytical model simulation time was 11 times less than the numerical model (analytical and numerical simulation times are 19 and 213, respectively) for the studied motor in computer with 32-GB RAM and TM i7-7700 Processor.

Recently Rahideh et al. [28] presented a 2-D analytical model for the permanent magnet single-sided linear motors (PMSSLMs) in which the UMF was introduced as one of the main challenges in these motors and the best case had 317 N for this component. However, in the proposed double-sided linear motor these normal forces are eliminated due to attraction between PMs, primary and secondary stators.

Also, it can be helpful to provide a simple comparison between the design specifications of the SDOPML and PMSSLM in the same volume. Table 5 shows this comparison, and the normal force components in both single-sided and double-sided structures have been determined.

Table 5. Design specifications of the proposed SDOPML and PMSSLM.

(a): SDOPML

	Parallel	Ideal Halbach	2-segment Halbach	Bar magnet in the shifting direction
Tangential force (N)	57.42	58.11	59.35	48.51
Unbalance force (N)	0.00	0.00	0.00	0.00
Nominal current (rms) (A)	3.57	3.57	3.57	3.57
Nominal speed (m/s)	1.00	1.00	1.00	1.00
Induced voltage (rms) (V)	6.12	6.23	6.14	6.07
Output power (w)	57.42	58.11	59.35	52.51
Losses (w)	13.46	12.52	11.93	13.67
Efficiency %	81.23	82.27	83.26	79.34

(b): PMSSLMs

	Parallel	Ideal Halbach	2-segment Halbach	Bar magnet in the shifting direction
Tangential force (N)	60.00	60.00	63.24	51.73
Unbalance force (N)	446.00	441.00	481.00	317.00
Nominal current (rms) (A)	3.57	3.57	3.57	3.57
Nominal speed (m/s)	1.00	1.00	1.00	1.00
Induced voltage (rms) (V)	6.61	6.65	6.43	6.13
Output power (w)	60.00	60.00	63.20	51.71
Losses (w)	12.13	11.22	10.91	11.80
Efficiency %	83.18	84.24	85.27	81.42

5. CONCLUSION

In this paper, an accurate 2-D analytical model that is generic and applicable for the arbitrary number of phases and pole-pairs has been presented for a slotless double-sided outer-armature permanent-magnet linear motor. The sub-domain method was utilized to predict the magnetic flux density components for each sub-region. The analytically extracted magnetic flux density components were applied to determine the machine quantities such as self and mutual inductances, induced voltage, and force components by considering different magnetization patterns (i.e., Parallel, ideal Halbach, 2-segment Halbach and bar magnet in shifting direction magnetization patterns). The accuracy of the obtained 2-D analytical model was confirmed by 2-D FEM. The benefit of the simulation time in the proposed analytical model

against the FEM was realized, and the analytical model took about one-eleventh of the time compared with the FEM. Other observable results were:

- Both side magnetization patterns formed the flux path, and it is possible to eliminate mover core or replacing it by other materials to reduce cost or obtaining lighter motor including less volume.
- Comparison between the proposed double-sided PM linear motor and the single-sided one with the same volume and same input reveals that in the double-sided case the output efficiency decreases slightly while the double-sided structure removes the normal force component.
- The output tangential forces have a linear relation with the input currents, and these currents have no effects on the normal force component.
- Halbach magnetization patterns reduce the output disturbance, which means that the induced voltage in the winding includes less harmonics in the case of Halbach magnetization patterns.

6. LIST OF SYMBOLS AND ABBREVIATIONS

Variables and parameters:

I_k	Input peak current
θ_k	Phase shift of kth harmonic of the phase currents
v	Velocity of the mover
p	Number of pole pairs
L_x	Stator length
$\mathbf{J}$	Current density vector
τ_p	Pole pitch
N_t	Number of each coil turn
n	spatial harmonic orders
y_0	Interface between the mover and PMs sub-regions
y_1	Interface between the PMs and air-gap sub-regions
y_2	Interface between the air-gap and winding sub-regions
y_3	Interface between the winding and stator sub-regions
y_4	Interface between the stator and stator exterior sub-regions
μ_0	Free space permeability
$\mathbf{M}$	Magnetization vector of PMs
M_x	Tangential components of the magnetization vector
M_y	Normal components of the magnetization vector
B_{rem}	PM remanence
τ_m	Each PM width
k_x	x-direction magnetized PM width to the pole pitch
k_y	y-direction magnetized PM width to the pole pitch
N_c	Number of coils in each phase
L_z	Length of motor along z-direction (motor depth)
k	Number of input current harmonics
x_1	Middle position of the coil-side
x_2	Middle position of the coil-side
I_i	Input current of the ith phase
q	Number of phases
d	Mover displacement
d_0	Initial position of the mover
t	Time
μ_r^s	Stator relative permeability
μ_r^m	Mover relative permeability
μ_r^{pm}	PMs relative permeability
K_f	Filling factor

Output definitions:

$\mathbf{A}$	Magnetic vector potential
B_x	Tangential component of the magnetic flux density
B_y	Normal component of the magnetic flux density
B_x^{pa}	Tangential component of the magnetic flux density in the primary air-gap
B_y^{pa}	Normal components of the magnetic flux density in the primary air-gap
B_x^{sa}	Tangential component of the magnetic flux density in the secondary air-gap
B_y^{sa}	Normalcomponent of the magnetic flux density in the secondary air-gap
B_y^w	The normal component of the magnetic flux density in the winding
λ_i^{pm}	linked Flux with the ith phase originated by only PMs
λ_i^w	linked Flux with the ith phase winding due to only ith phase current
λ_{ij}^w	linked Flux with the jth phase due to the ith phase current
L_{ii}	self-inductance of the ith phase
L_{ij}	Mutual inductance between ith and jth phases
E_i	Induced voltage in the ith phase due to PMs
F_x	Tangential component of the electromagnetic force
F_y	Normalcomponent of the electromagnetic force

REFERENCES

1. Yan, L., J. Peng, Z. Jiao, C. Y. Chen, and I. M. Chen, "Flux field and thrust analysis of permanent magnet linear machines with isolated movers," *IEEE Transaction on Magnetics*, Vol. 52, No. 8, Article Number: 8203208, 2015.
2. Kim, S. A., T. U. Zhu, S. G. Lee, S. Saha, and Y. H. Cho, "Electromagnetic normal force characteristics of a permanent magnet linear synchronous motor with double primary side," *IEEE Transaction on Magnetics*, Vol. 50, No. 1, Article Number: 4001204, 2014.
3. Virtic, P. and B. Stumberger, "Analytical analysis of magnetic field and force calculation in a slotless-type permanent magnet linear synchronous machine; Verification with numerical analysis," *Electric Machines & Drives Conference*, Vol. 2, 963–968, 2017.
4. Azzouzi, J., G. Barakat, and B. Dakyo, "Quasi-3-D analytical modeling of the magnetic field of an axial flux permanent-magnet synchronous machine," *IEEE Transactions on Energy Conversion*, Vol. 20, No. 4, 746–752, 205.
5. Guo, R., H. Yu, T. Xia, Z. Shi, W. Zhong, and X. Liu, "A simplified subdomain analytical model for the design and analysis of a tubular linear permanent magnet oscillation generator," *IEEE Access*, Vol. 6, 42355–42367, 2018.
6. Kang, G. H., J. P. Hong, and G. T. Kim, "A novel design of an air-core type permanent magnet linear brushless motor by space harmonics field analysis," *IEEE Transactions on Magnetics*, Vol. 37, No. 5, 3732–3736, 2001.
7. Vaez-Zadeh, S. and A. H. Isfahani, "Multiobjective design optimization of air-core linear permanent-magnet synchronous motors for improved thrust and low magnet consumption," *IEEE Transactions on Magnetics*, Vol. 42, No. 3, 446–452, 2006.
8. Anglada, J. R., S. M. Sharkh, and M. A. Yuratich, "Calculation of rotor losses in PM machines with retaining sleeves using transfer matrices," *IET Electric Power Appl.*, Vol. 12, No. 8, 1150–1157, 2018.
9. Vaez-Zadeh, S. and A. Isfahani, "Enhanced modeling of linear permanent-magnet synchronous motors," *IEEE Transactions on Magnetics*, Vol. 43, No. 1, 33–39, 2007.
10. Teymoori, S., A. Rahideh, H. Moayed-Jahromi, and M. Mardaneh, "2-D analytical magnetic field prediction for consequent-pole permanent magnet synchronous machines," *IEEE Transactions on Magnetics*, Vol. 52, No. 6, Article Number: 8202114, 2016.
11. Guo, B., Y. Huang, F. Peng, Y. Guo, and J. Zhu, "Analytical modeling of manufacturing imperfections in double-rotor axial flux PM machines: Effects on back EMF," *IEEE Transactions on Magnetics*, Vol. 53, No. 6, Article Number: 7200605, 2017.

12. Ramakrishnan, K., M. Curti, D. Zarko, G. Mastinu, J. J. H. Paulides, and E. A. Lomonova, "Comparative analysis of various methods for modelling surface permanent magnet machines," *IET Electric Power Applications*, Vol. 11, No. 4, 540–547, 2017.
13. Dai, X., Q. Liang, J. Cao, Y. Long, J. Mo, and S. H. Wang, "Analytical modeling of axial-flux permanent magnet eddy current couplings with a slotted conductor topology," *IEEE Transactions on Magnetics*, Vol. 52, No. 2, Article Number: 8000315, 2016.
14. Kwon, Y. S. and W. J. Kim, "Steady-state modeling and analysis of a double-sided interior permanent-magnet flat linear brushless motor with slot-phase shift and alternate teeth windings," *IEEE Transactions on Magnetics*, Vol. 52, No. 11, Article Number: 8205611, 2016.
15. Yin, X., Y. Fang, X. Huang, and P. D. Pfister, "Analytical modeling of a novel vernier pseudo-direct-drive permanent-magnet machine," *IEEE Transactions on Magnetics*, Vol. 53, No. 6, Article Number: 7207404, 2017.
16. Liu, X., H. Hu, J. Zhao, A. Belahcen, and L. Tang, "Armature reaction field and inductance calculation of ironless BLDC motor," *IEEE Transactions on Magnetics*, Vol. 52, No. 2, Article Number: 8200214, 2016.
17. Kazerooni, K., A. Rahideh, and J. Aghaei, "Experimental optimal design of slotless brushless pm machines based on 2-D analytical model," *IEEE Transactions on Magnetics*, Vol. 52, No. 5, Article Number: 8103116, 2016.
18. Ko, Y., J. Song, M. Seo, W. Han, Y. Kim, and S. Jung, "Analytical method for overhang effect of surface-mounted permanent-magnet motor using conformal mapping," *IEEE Transactions on Magnetics*, Vol. 54, No. 11, Article Number: 8208005, 2018.
19. Liu, X., H. Hu, J. Zhao, A. Belahcen, L. Tang, and L. Yang, "Analytical solution of the magnetic field and EMF calculation in ironless BLDC motor," *IEEE Transactions on Magnetics*, Vol. 52, No. 2, Article Number: 8100510, 2016.
20. Shin, K. H., H. W. Cho, S. H. Lee, and J. Y. Choi, "Armature reaction field and inductance calculations for a permanentmagnet linear synchronous machine based on subdomain model," *IEEE Transactions on Magnetics*, Vol. 53, No. 6, Article Number: 8105804, 2017.
21. Brahim, L.-C., K. Boughrara, and R. Ibtiouen, "Cogging torque minimization of surface-mounted permanent magnet synchronous machines using hybrid magnet shapes," *Progress In Electromagnetics Research B*, Vol. 62, 49–61, 2015.
22. Zhu, Z. Q., D. Ishak, D. Howe, and J. Chen, "Unbalanced magnetic forces in permanent-magnet brushless machines with diametrically asymmetric phase windings," *IEEE Transactions on Industry Applications*, Vol. 43, No. 6, 1544–1553, 2007.
23. Yao, Y., Q. Lu, X. Huang, and Y. Ye, "Fast calculation of detent force in PM linear synchronous machines with considering magnetic saturation," *IEEE Transactions on Magnetics*, Vol. 53, No. 6, Article Number: 8102404, 2017.
24. Vahaj, A. A., A. Rahideh, and T. Lubin, "General analytical magnetic model for partitioned-stator flux-reversal machines with four types of magnetization patterns," *IEEE Transactions on Magnetics*, 2019, DOI: 10.1109/TMAG.2019.2929477.
25. Ghaffari, A., A. Rahideh, H. Moayed-Jahromi, A. A. Vahaj, A. Mahmoudi, and W. L. Soong, "2-D analytical model for outer-rotor consequent-pole brushless PM machines," *IEEE Transactions on Energy Conversion*, 2019, DOI: 10.1109/TEC.2019.2941935.
26. Boutora, Y., N. Takorabet, and R. Ibtiouen, "Analytical model on real geometries of magnet bars of surface permanent magnet slotless machine," *Progress In Electromagnetics Research B*, Vol. 66, 31–47, 2016.
27. Zhang, Y., Z. Yang, M. Yu, K. Lu, Y. Ye, and X. Liu, "Analysis and design of double-sided air core linear servo motor with trapezoidal permanent magnets," *IEEE Transactions on Magnetics*, Vol. 47, No. 10, 3236–3239, 2011.
28. Rahideh, A., A. Ghaffari, A. Barzegar, and A. Mahmoudi, "Analytical model of slotless brushless PM linear motors considering different magnetization patterns," *IEEE Transactions on Energy Conversion*, Vol. 33, No. 4, 1797–1804, 2018.